Applied Catalysis A: General 511 (2016) 78–86

Contents lists available at ScienceDirect

Applied Catalysis A: General

journal homepage: www.elsevier.com/locate/apcata

Catalyst structure and substituent effects on epoxidation of styrenics with immobilized Mn(tmtacn) complexes

Patricia Anne A. Ignacio-de Leon[1], Christian A. Contreras[2], Nicholas E. Thornburg, Anthony B. Thompson[3], Justin M. Notestein*

Department of Chemical and Biological Engineering, Northwestern University, 2145 Sheridan Road, Evanston, IL 60208, USA

ARTICLE INFO

Article history:
Received 14 August 2015
Received in revised form
30 November 2015
Accepted 1 December 2015
Available online 3 December 2015

Keywords:
Epoxidation
Hydrogen peroxide
Supported catalyst
Hammett relationships
Manganese

ABSTRACT

Monomeric and dimeric complexes of Mn 1,4,7-trimethyl-1,4,7-triazacyclononane (tmtacn) were immobilized under reaction conditions onto solid supports to create heterogeneous catalysts for epoxidation with H_2O_2. These solid supports consist of activated carbon or silica grafted or co-condensed with benzoic or C3/C4 acids that function both as tethering points and as required co-catalysts. Immobilized catalysts were as much as 50-fold faster than the analogous soluble system, and an immobilized, dimeric Mn(tmtacn) complex with a solid benzoic acid co-catalyst gave the highest yields to epoxide. A Hammett study on the catalytic epoxidation of a series of styrenes showed weak increases in yield for more electron-withdrawing *p*-substituents reactants for both immobilized complexes, which runs counter to previous observations with analogous homogeneous catalysts, and which appears to reflect a previously unappreciated tradeoff between the intrinsic epoxidation reactivity and strong catalyst inhibition by styrene oxides and glycols. Finally, these catalysts were tested with a variety of solid-co-catalysts, and were successfully utilized in the challenging epoxidation of divinylbenzene to industrially-useful divinylbenzene dioxide using a cascade of two catalyst charges.

1. Introduction

The selective oxidation of alkenes to epoxides or *cis*-diols remains an important research area for catalyst development and industrial use. Epoxides and vicinal diols are versatile and reactive chemical intermediates for commodity chemicals and fine/specialty chemicals alike. Dioxides (bisepoxides) such as divinylbenzene dioxide have particular application in epoxy resins, but their syntheses see very little research in the open literature. Alkene epoxidation/*cis*-dihydroxylation has been achieved using a wide variety of oxygen-transfer agents including H_2O_2, organic peroxides (e.g., *t*-BuOOH) [1], and organic peroxyacids (e.g., *m*-chloroperbenzoic acid) [2], and facilitated by small molecule inorganic and organocatalysts [3]. H_2O_2 is a preferred oxidant due to its low cost, high atom efficiency and environmentally benign co-product (water) [4–6]. Transition metal-containing epoxidation catalysts include salen [7–10] or porphyrin [11–13] complexes, and a class that takes inspiration from non-heme metalloenzymes and consists of Fe or Mn complexes of ligands including triazacyclononane (tacn) [14], tris(2-pyridylmethyl) amine (tpa) [15,16], bis(2-pyridylmethyl) ethylenediamine (bpmen) [17] and others [18–21].

Manganese 1,4,7,-trimethyl-1,4,7-triazacyclononane (tmtacn) complexes were first prepared and characterized in 1988 by Weighardt et al., [22]. and these and related triazacyclononane (tacn) complexes have been reported and reviewed [23,24] for olefin epoxidation and dihydroxylation [25–27], alcohol oxidation [28–31], sulfoxidation [32,33], and alkane oxidation [34–36] to alcohols, aldehydes and ketones via organic hydroperoxides [37]. Carboxylic acid co-catalysts are essential to achieve high catalyst productivity and selectivity [38–44], and the acids have been proposed to form adducts with the Mn complex [45,46].

Immobilized versions of this catalyst have attracted interest due to ease of catalyst (or co-catalyst) separation [47–50]. Mn(IV) complexes have been covalently attached to insoluble polymers by *N*-alkylation of tacn [51], or immobilized as insoluble salts with polyoxometallates [52]. Our group has previously reported on immobilization of the dimer [Mn(tmtacn)-(μ-O)$_3$-Mn(tmtacn)] Mn_2 under reaction conditions onto the surface of carboxylic acid-

* Corresponding author at: 2145 Sheridan Rd., Technological Institute E136, Evanston, IL 60208, USA.
E-mail address: j-notestein@northwestern.edu (J.M. Notestein).
[1] Argonne National Laboratory, Energy Sciences Division, USA.
[2] GreatPoint Energy, USA.
[3] University of Minnesota, Department of Chemistry, USA.

http://dx.doi.org/10.1016/j.apcata.2015.12.002
0926-860X/

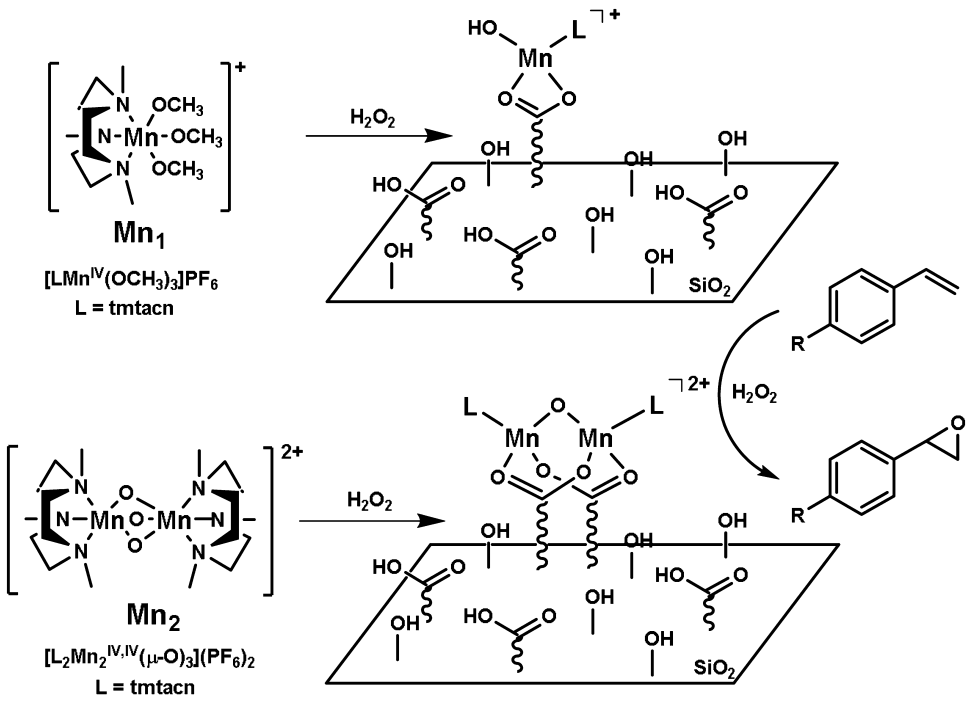

Scheme 1. The complexes **Mn**$_1$ and **Mn**$_2$ used in this study and a representation of the immobilized catalysts for the epoxidation of *p*-substituted styrenes[a].
[a]The structure of immobilized **Mn**$_2$ has been established earlier as a reduced $Mn^{III,III}$ carboxylate-bridged dimer [14]; the Mn—O—Mn bond will open under reaction conditions. The structure of immobilized **Mn**$_1$ is proposed by analogy. Counteranions not shown. Supports include a silyl benzoate and a silyl propanoate grafted to SiO_2 and a butanoate species co-condensed into a SiO_2 framework.

modified solid supports (Scheme 1), and we have carried out epoxidation screening with diverse alkenes [53], and several solid supports [54]. Spectroscopic [14] and microkinetic modeling studies [55] are consistent with formation of dimeric Mn complexes with bridging carboxylates as the catalytic resting state, and a Mn hydroperoxo active intermediate, as has been argued by others [40].

Utilization of Mn(tacn) catalysts has overwhelmingly focused on the dimeric complexes, even though a mononuclear active species [56]. has been proposed to be produced from the dimer. Likewise, unusual reactivity of an immobilized Mn(tacn) was proposed to be due to stabilization of a monomeric structure [47]. However, there are relatively few reports on the direct utilization of monomers or systematic studies of the effect of alkene and catalyst structure, especially for solid-supported systems. Ilyashenko et al. recently compared Mn_1 and Mn_2 as homogeneous catalysts and suggested unique catalytic active species for each, as evidenced by a marked difference in reactivity patterns towards various alkenes [57]. In this new contribution, monomeric and dimeric Mn precursor complexes Mn_1 and Mn_2 are immobilized on several different solid co-catalysts and studied in the epoxidation of a family of *p*-substituted styrenes with varying electron density (Scheme 1). In addition to mechanistic insight, these results are valuable for optimizing reaction conditions over this important class of catalysts, which we demonstrate for the challenging reaction of divinylbenzene (DVB) epoxidation, as relevant to the synthesis of epoxy resins.

2. Experimental

2.1. General considerations

N_2 sorption experiments were performed with a Micromeritics ASAP 2010. Diffuse reflectance, fourier transform-infrared spectroscopy (DRIFTS) was performed with a Nexus 870 spectrometer (Thermo Nicolet). ^{13}C NMR (CP-MAS) spectra for solid samples were collected with a Varian 400 MHz VNMRS. Elemental analyses were carried out by Galbraith Laboratories. Electrospray ionization mass spectrometry (ESI-MS) was carried out in the positive ion mode using a Bruker AmaZon SL Ion Trap. Scanning electron microscopy (SEM) used a Hitachi S4800-II cFEG SEM.

2.2. Catalyst synthesis

1,4,7-Trimethyl-1,4,7-triazacyclononane (tmtacn) was synthesized in several steps of tosylation, cyclization, and reductive amination following literature procedures to give a viscous, light yellow oil whose ^1H NMR spectra agreed with literature (overall 18% yield) [58]. [Mn(tmtacn)(OMe)$_3$](PF$_6$) (Mn_1) was synthesized according to published methods and collected as dark brown needles (10% yield) [26]. Mass spectrum (ESI^+): *m*/*z* 319.17 ($[M-PF_6]^+$). Elemental analysis (calc. $MnC_{12}H_{30}N_3O_3PF_6$): C 31.1% (31.0), N 8.9% (9.0), H 6.6% (6.5), Mn 14% (11.8). [Mn_2(tmtacn)$_2$(μ-O)$_3$](PF$_6$)$_2$ (**Mn**$_2$) was synthesized via modification of a known procedure and collected as red crystals (59% yield) [22]. Mass spectrum (ESI^+): *m*/*z* 645.17 ($[M-PF_6]^+$). Elemental analysis (calc. $Mn_2C_{18}H_{44}N_6O_4P_2F_{12}$): C 26.9% (26.7), N 10.3% (10.4), Mn 13.0% (13.6).

2.3. Co-catalyst synthesis

Silica-based solid co-catalysts were prepared by grafting or co-condensation. Prior to surface modification, a commercially available mesoporous SiO_2 (Selecto brand, 32–63 μm particle size) was pre-treated by heating to 150 °C under dynamic vacuum for 12 h. Grafted co-catalysts were prepared as previously reported at nominal loadings of 0.25, 0.5 or 1 mmol/g from grafting of 2-(carbomethoxy) ethyltrimethoxysilane or ethyl 4-(triethoxysilyl) benzoate to dehydrated SiO_2 in pyridine. After reflux and washing, the free acids were generated by refluxing in 1 M HCl and washing to yield propanoic acid- and benzoic acid-modified silica (PA-SiO_2 and BA-SiO_2), respectively [54]. Sol–gel materials were

prepared via co-condensation of tetraethyl orthosilicate and 3-cyanopropyltriethoxysilane in a mixture of ethanol, water and *n*-dodecylamine [59]. Carboxylic acids were afforded by subsequent nitrile hydrolysis in aqueous H_2SO_4 at reflux conditions [60–63]. All samples were dried under dynamic vacuum prior to further use. Actual organic loadings in the hybrid SiO_2 materials were quantified by TGA, as detailed below. Carbon (C, Calgon brand, granular, <1000 μm) was treated with 2 M HCl then rinsed with 18 MΩ water, ethanol and ether. Acid-treated carbon (AC) was obtained by further treatment with 5 M HNO_3, followed by copious rinsing with 18 MΩ water [54]. See the supporting information for full details on molecular and materials syntheses.

2.4. Epoxidation of p-substituted styrenes

Styrene (≥99.0%, ReagentPlus, Sigma–Aldrich), styrene oxide (97%, Aldrich), 4-methylstyrene (≥99.0%, 0.005% 4-*tert*-butylcatechol as stabilizer, Aldrich), 4-vinylanisole (97%, Aldrich), 4-cyanostyrene (97%, stabilized with 0.05% 4-*tert*-butylcatechol, Alfa Aesar), 4-trifluoromethylstyrene (98%, contains 0.1% 4-*tert*-butylcatechol as inhibitor, Aldrich), divinylbenzene (DVB, 80%, technical grade, 1000 ppm *tert*-butylcatechol as inhibitor, Aldrich), anisole (anhydrous, 99.7%, Sigma–Aldrich), and benzonitrile (anhydrous, >99%, Sigma–Aldrich), were passed through an activated alumina column in order to remove inhibitors and other imputities and were stored at 2–6 °C until use. Acetonitrile (Spectrophotometric grade, 99.7+%, Alfa Aesar), 1,2-dichlorobenzene (99%, Alfa Aesar), 3-chloroperoxybenzoic acid (77% max., Aldrich), H_2O_2 (30 wt% in water, ACS reagent, Sigma–Aldrich) and Ag (powder, <250 μm, 99.99% trace metals basis, Aldrich) were used as received. Standard catalytic tests were performed at 0 °C at 3000:1000:1:10 H_2O_2: C=C: complex: carboxylate mole ratios. Note that the catalyst was added based on moles of the complex and alkene based on moles of the double bond; thus, reactions with $\mathbf{Mn}_2$ contain twice as many Mn atoms as for reactions using $\mathbf{Mn}_1$ and reactions with DVB contain half as many moles of the substituted styrene as for the other reactants. 1,2-Dichlorobenzene was used as an internal standard.

In a standard reaction, a measured amount of the carboxylic acid-modified SiO_2 was added to a vial equipped with a stir bar, followed by 2.5 mL of 0.4 mM $\mathbf{Mn}_1$ or $\mathbf{Mn}_2$ in acetonitrile. The mixture was allowed to equilibrate for 40 min at 0 °C with stirring on a cold plate, after which 7.5 mL of a 0.15 M alkene solution in acetonitrile was added. Timing commenced upon addition of 0.7 mL of a solution of dry H_2O_2 in acetonitrile (prepared by diluting 10 mL 30% aqueous H_2O_2 with 20 mL acetonitrile containing 7 g anhydrous $MgSO_4$ followed by decanting the supernatant). Aliquots were withdrawn through a Whatman GF/F syringe filter at certain time points over a 24 h interval and delivered to GC vials containing approximately 10 mg Ag powder to consume any unreacted H_2O_2 and stabilize the oxygenates prior to GC–MS analysis. Analyte concentrations were quantified with a Shimadzu GCMS-QP2010 SE on a Phenomenex ZB-624 capillary column (30m × 0.25 mm diameter × 1.4 μm thickness) based from prepared calibration standards of 0–5 mM analyte in acetonitrile. *p*-X-styrenes, styrene oxide, 1-phenyl-1,2-ethanediol, benzaldehyde, phenylacetaldehyde, acetophenone and divinylbenzene were calibrated against commercially available standards. Ethylvinylbenzene monoxide (EVBMO), divinylbenzene monoxide (DVBMO) and divinylbenzene dioxide (DVBDO) were calibrated against authentic samples obtained as a gift. Calibration standards for *p*-X-styrene oxides were prepared from epoxidation with excess m-chloroperbenzoic acid.

3. Results and discussion

3.1. Characterization of acid-modified SiO_2

Commercially available mesoporous SiO_2 gel particles are modified by grafting silane esters from a colloidal mixture in pyridine, followed by hydrolysis (Scheme 2). The overall particle morphology is maintained by SEM (Supporting information Fig. S1) after grafting. Solid-state ^{13}C CP/MAS NMR (Supporting information Table S1) shows resonances at 6, 27, and 177 pm for the final grafted acid, with loss of a resonance at 50 ppm from the intermediate methyl ester, supporting the successful covalent anchoring of the organosilanes, and IR spectra for unmodified and functionalized samples illustrate the appearance of new peaks corresponding to carbonyl and alkyl stretches at ca. 1700 and 2900 cm^{-1}, respectively (Supporting information Fig. S2).

N_2 physisorption on the solid co-catalysts (Supporting information Fig. S3) gives surface areas from the BET model and pore dimensions from the BJH model (Table 1). The grafted materials remain mesoporous but show small decreases in surface area and pore diameter relative to the parent SiO_2, as expected for sub-monolayer coverage of the organosilanes. The co-condensed material used is also mesoporous, while the carbon sample has bimodal porosity. TGA quantifies the loss of organics during combustion of the solid co-catalysts to estimate carboxylate molar loadings (Supporting information Fig. S4). All samples are white in color after heat treatment to 800 °C in O_2, consistent with complete combustion of the organics. Mass loss occurs between 350 and 550 °C. Loadings (mmol/g) and average surface densities (groups/nm^2) are given in Table 1 and are calculated assuming loss of a surface $C_3H_5O_2$ fragment for PA-SiO_2, $C_7H_5O_2$ for BA-SiO_2, and $C_4H_7O_2$ for the sol–gel material. Overall, the loadings, pore structures, and functional group assignments for the supports are very comparable to similar materials reported by some of us in previous studies [54]. A detailed analysis of the Mn_2-modified materials has also been previously carried out [14].

3.2. Catalytic epoxidation of styrene

Fig. 1 shows typical kinetic profiles for the first 2 h of the epoxidation of styrene with H_2O_2 using $\mathbf{Mn}_1$ and $\mathbf{Mn}_2$ supported on BA-SiO_2 and PA-SiO_2. In all cases, the highest available loadings of BA-SiO_2 and PA-SiO_2 were used, 0.87 and 0.42 mmol/g. Styrenics are well-studied benchmark reactants, [64]. which also allow for investigation of rate dependence on the nature of the alkene via standard Hammett analyses [65,66]. In many cases, these catalysts exhibit a ~15 min induction period following H_2O_2 addition. We and others have documented this induction period and attribute it to assembly of the catalyst–carboxylate complex [53,67]. Major products styrene oxide and styrene diol, and rearrangement/overoxidation products phenylacetaldehyde and benzaldehyde (presumably from oxidative cleavage, Scheme 3) increase monotonically in concentration for 300–450 min, after which product concentrations generally plateau. See the supporting information for full kinetic traces out to 24 h (Supporting information Fig. S5). Interestingly, $\mathbf{Mn}_1$/BA-SiO_2 shows has an initial epoxidation rate that is <10% that of $\mathbf{Mn}_1$/PA-SiO_2, but its productivity remains steady up to and past 450 min, ultimately leading to high yields. Fig. 1 shows only total product, since selectivity to epoxide exceeded 90% in all cases. Mass balance, expressed as the total mmol of all observed products relative to mmol consumed alkene, is >95%, demonstrating that all key products are accounted for by this analysis.

Table 2 gives the initial rates and total turnover numbers (TON, mole product per mole of $\mathbf{Mn}_1$ or $\mathbf{Mn}_2$, not per Mn atom) and product selectivity at 24 h. Initial rates are calculated from sustained

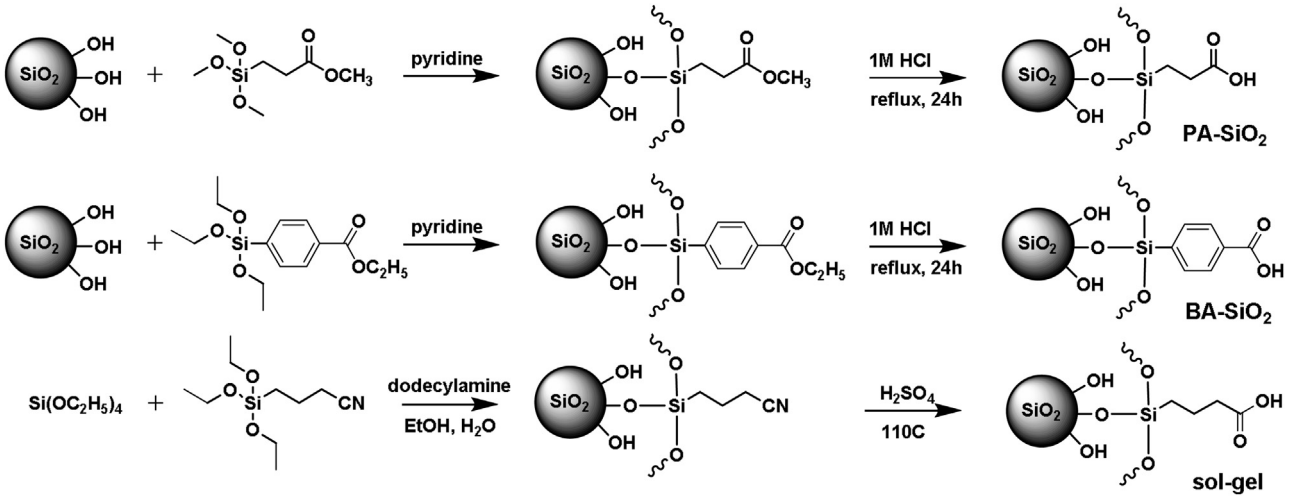

Scheme 2. Reaction schemes for modifying SiO_2 with carboxylic acids[a].
[a]Grafting yields PA-SiO_2 and BA-SiO_2 and co-condensation of tetraethoxysilane (TEOS) and 3-cyanopropyltriethoxysilane (CPTES) with subsequent nitrile hydrolysis gives the carboxylic acid-containing "sol–gel" material.

Table 1
Solid support and co-catalyst properties.

Co-catalyst	Loading[a] (mmol/g)	Grafting density (nm^{-2})[b]	Surface area (m^2/g)[b]	Pore diameter (nm)[b]
SiO_2	–	–	650	6.0
PA-SiO_2[c]	0.87	0.83	475	5.5
PA-SiO_2	0.47	0.45	475	5.5
PA-SiO_2	0.32	0.31	475	5.5
BA-SiO_2[c]	0.42	0.44	560	5.6
BA-SiO_2	0.27	0.29	550	5.6
sol–gel[c]	3.5	3.9	575	3.9
C[c]	n/a	n/a	2200	3.6, 1.6

[a] Calculated loadings (mmol/g) from thermogravimetric analyses.
[b] Surface areas and average pore diameters calculated from N_2 physisorption isotherms.
[c] Used for catalystic testing described below.

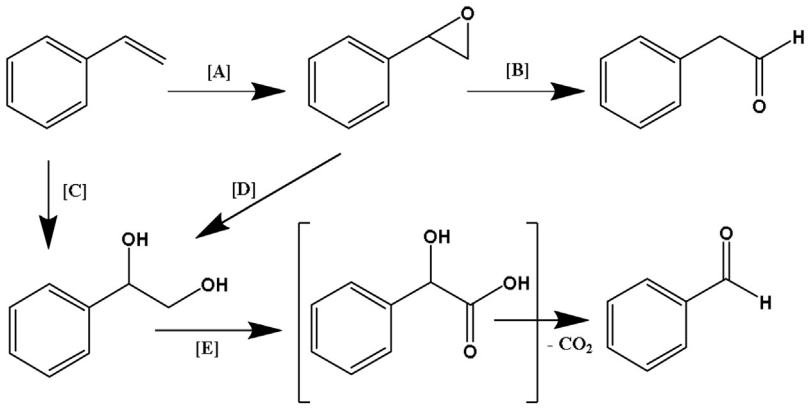

Scheme 3. Possible reaction networks in styrene oxidation[a].
[a]Direct epoxidation pathway [A], rearrangement to phenylacetaldehyde [B], styrene diol formation either by [C] direct dihydroxylation or by [D] epoxide hydrolysis, and [E] oxidative cleavage to benzaldehyde via an unobserved α-hydroxy-carboxylic acid [72].

initial rates and neglect induction periods of ~15 min in most cases. As expected, yields are negligible in the absence of H_2O_2 and are not shown. While the system turns over with only **Mn**$_1$ or **Mn**$_2$ and H_2O_2 (base case, entries 5 and 6), a carboxylic acid co-catalyst appreciably boosts initial rates (entries 2, 4, 10) except for the combination of **Mn**$_2$ and propanoic acid (entry 8), which is not effective at these levels. Relatively weak alkanoic acids have previously been shown to be poor co-catalysts for **Mn**$_2$ at these conditions [67]. In spite of increased rates, the soluble benzoic and propanoic acid co-catalysts give little improvement to overall yields vs. the base case. In contrast, the solid co-catalysts significantly outperform the soluble system in both yield and initial rate, in agreement with earlier reports from our group [14,53,54]. For either **Mn**$_1$ or **Mn**$_2$, the solid PA-SiO_2 gives a remarkable 50-fold increase in initial rate relative to soluble PA. The high rate of the **Mn**$_1$/PA-SiO_2 system is accompanied by a negligible induction period. Because the induction period has been ascribed to the formation of the active catalyst [53], it appears likely that the smaller **Mn**$_1$ and the flexible co-catalyst enables more rapid complex formation than for any other combination. For **Mn**$_2$, the solid co-catalysts give a 5–7-fold increase

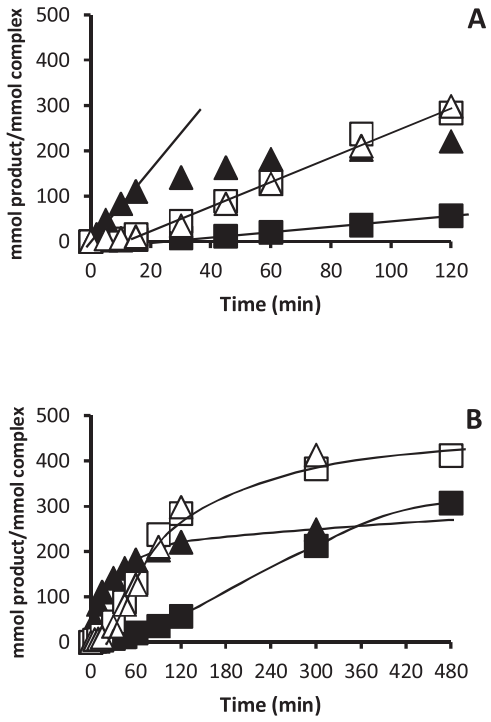

Fig. 1. Representative kinetic profiles for the first 2 h (A) and 8 h (B) of conversion of styrene into oxidation products (sum of styrene oxide, styrene diol, phenylacetaldehyde, and benzaldehyde) with **Mn**$_1$/BA-SiO$_2$ (■), **Mn**$_2$/BA-SiO$_2$ (□), **Mn**$_1$/PA-SiO$_2$ (▲) and **Mn**$_2$/PA-SiO$_2$ (△). Note that the traces for **Mn**$_2$/BA-SiO$_2$ and **Mn**$_2$/PA-SiO$_2$ are nearly superimposed. Epoxide selectivity exceeds 90% over this time range. Curves are guides to the eye showing initial rates in A and the overall time course of reaction in B.

Table 2
Summary of turnovers, selectivity (% epoxide) and initial rates for styrene oxidation with H_2O_2 with several catalytic systems.[a]

Entry		Ton[b]	% Epoxide[c]	Initial rate[d]
1	Mn_1/PA-SiO_2	287	91	7.5
2	Mn_1/PA	106	98	0.16
3	Mn_1/BA-SiO_2	358	86	0.67
4	Mn_1/BA	88	97	0.55
5	Mn_1	74	96	0.09
6	Mn_2	77	96	0.05
7	Mn_2/PA-SiO_2	515	91	2.9
8	Mn_2/PA	77	96	0.05
9	Mn_2/BA-SiO_2	405[e]	98	2.46
10	Mn_2/BA	59	99	0.36

[a] Reaction conditions: 0.1 M styrene, 0.1 mM **Mn**$_1$ or **Mn**$_2$, 0.3 M dried H_2O_2/MeCN, 10:1 supported acid:Mn complex, 0 °C in MeCN for 24 h.
[b] TON=(total mmol products observed/mmol **Mn**$_1$ or **Mn**$_2$) at t = 24 h.
[c] % Epoxide = (mmol epoxide/total mmol products observed) × 100 at t = 24 h.
[d] Initial rate (TON/min) from initial linear trend excluding any induction period.
[e] Yield at maximum, near 8 h.

in yields relative to the soluble case, while the enhancement is 3–4-fold for **Mn**$_1$. These performance enhancements are thought to be due to an effective higher concentration of the carboxylates on the surface, leading to more of the Mn complexes being present in their catalytically active form, coordinated to the carboxylates. The SiO_2 surface may also make the supported carboxylates more acidic through delocalization of the proton; increased acidity has been correlated by others with increased reactivity [40,67]. We have previously shown no evidence for catalytic activity in the solution above the solid [14,53,54], verifying that the active form of the catalyst is effectively immobilized under reaction conditions.

Product distributions are similar for all entries, suggesting that all combinations use a similar catalytic mechanism. In solution, the

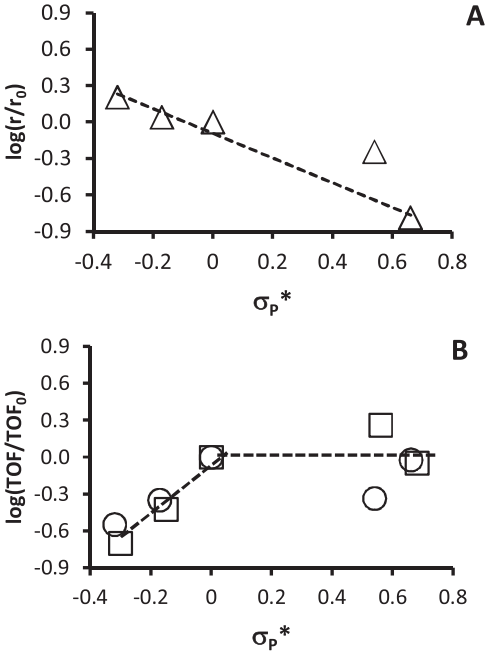

Fig. 2. Hammett [65] plots for *p*-substituted styrene epoxidation with (A) *m*-chloroperbenzoic acid and with H_2O_2 (B) as catalyzed by **Mn**$_1$/BA-SiO_2 (○) and **Mn**$_2$/BA-SiO_2 (□). Initial rates are expressed as mmol product/min and mmol product/(mmol **Mn**$_1$ or **Mn**$_2$)/min for oxidations with mCPBA and H_2O_2, respectively. Values for □ are offset by 0.02 units for clarity. Error bars are smaller than the symbols used for all runs.

stronger acidity of benzoic acid (pK_a 4.19 for benzoic acid vs. 4.86 for propanoic acid) [68] favors the formation of the Mn-carboxylate complex [67], leading to higher rates. On the surface, sterics and other factors may play an important role in determining the rate of active catalyst formation, and thus the initial rate of oxidation. The BA-SiO_2 co-catalyst is selected for further mechanistic investigation.

3.3. Alkene substituent effects

A Hammett series of *p*-substituted styrenes is studied to further investigate epoxidation with **Mn**$_1$ and **Mn**$_2$ catalysts. Alkene epoxidation in many systems, such as stoichiometric *m*-chloroperbenzoic acid (mCPBA) or Ti-SiO_2/ROOH, is accelerated for electron-rich alkenes [59,69]. Per expectations, a plot of (log) initial epoxidation rates vs. Hammett constants [65] (σ_p) for *p*-X-substituted styrenes (X = OMe, Me, H, CF_3, CN; larger σ_p indicates more electron-withdrawing) with mCPBA (Fig. 2A) has a reaction constant (slope) of ρ = -1.0. mCPBA is an electrophilic oxidant with which electron-rich methoxy- and methylstyrene are oxidized roughly an order of magnitude faster than the electron-poor cyanostyrene.

Initial oxidation rates for **Mn**$_1$/BA-SiO_2 and **Mn**$_2$/BA-SiO_2 are calculated as for Fig. 1, and typically include linear product evolution data often up to ~5 h, but exclude any initial induction period (typically ~15 min as has been observed for styrene). Error bars are calculated from at least two trials for each experiment. Table 3 summarizes TONs, initial rates and product selectivities for these *p*-substituted styrenes. The epoxide is the major product observed with all *p*-substituted styrenes, but *p*-X-benzaldehyde selectivity (proposed to be via the diol, see Scheme 3) is unusually high for the electron-donating X = OMe (22% for X = OMe cf. 1% for CF_3 and CN). There is also significant rearrangement into *p*-X-phenylacetaldehyde for the electron-withdrawing X = CF_3 (*ca.* 11% selectivity).

Table 3
Summary of TONs (mmol oxidation products/mmol complex) at $t = 5$ h for monofunctional *p*-substituted styrene oxidation with H_2O_2.

p-X-styrene	Hammett constant, σ_p[31]	Mn_1/BA-SiO_2		Mn_2/BA-SiO_2	
		TON[a] (% products)[b]	TOF[a]	TON[a] (% products)[b]	TOF[a]
X = OMe	−0.32	58 (69, 22, 9)	0.19	146 (75, 13, 4)	0.50
X = Me	−0.17	222 (94, 3, 3)	0.30	543 (96, 1, 3)	0.95
X = H	0	212 (86, 8, 6)	0.67	383 (98, 1, 1)	2.46
X = CF_3	0.54	932 (87, 1, 11)	0.31	1000 (89, 1, 10)	4.55
X = CN	0.66	765 (97, 1, 0)	0.64	1000 (98, 1, 1)	2.25

[a] mmol product/(mmol **Mn**$_1$ or **Mn**$_2$) or mmol product/(mmol **Mn**$_1$ or **Mn**$_2$)/min, extrapolated to zero time.
[b] Observed product distribution reported as % *p*-X-epoxide, % *p*-X-benzaldehyde, and % *p*-X-phenylacetaldehyde. Unreported diol is to balance, and <2% except for X = OMe with **Mn**$_2$/BA-SiO_2.

Table 4
Inhibitory effects on 4-cyanostyrene oxidation with **Mn**$_2$/BA-SiO_2.[a]

Additive	Initial rate[b]	K_I (M^{-1})[c]	TON
None	2.3	n/a	1000
0.1 M Benzonitrile	2.2	<0.5	1000
0.1 M Anisole	0.49	40	680
0.02 M Styrene oxide	0.07	1600	103
0.001 M Styrene diol	0.10	22,000	132

[a] Reaction conditions: 0.1 M 4-cyanostyrene, 0.1 mM **Mn**$_1$ or **Mn**$_2$, 0.3 M dried H_2O_2/MeCN, 10:1 supported acid:Mn center, 0 °C in MeCN for 24 h.
[b] mmol product/(mmol **Mn**$_1$ or **Mn**$_2$)/min.
[c] Approximate binding constant for inhibitors listed.

The dependence of the reaction rate on the alkene is similar for **Mn**$_1$/BA-SiO_2 and **Mn**$_2$/BA-SiO_2 for the majority of substrates. (Fig. 2, Table 3). Rates increase from X = OMe to X = Me to X = H, corresponding to an increase in the Hammett constant, and with a reaction constant (slope) of $\rho = +2.0$, which at face value indicates a nucleophilic oxidant. Product yields also increase, and TONs per **Mn**$_2$ complex are approximately double that of those per **Mn**$_1$ complex, giving a first indication that yields with certain reactants may be limited by poisoning of Mn atoms. Although there is some variability in the response to the X = CF_3 reactant, there is on average, no further rate increase to X = CN, even though there is a large increase in the Hammett constant. Likewise, yields increase, although the reaction reaches completion for the **Mn**$_2$ catalyst, limiting further comparisons. The trends seen in this Hammett study are quite unlike those of the soluble catalyst investigation of Ilyashenko et al. [57], where a strong dependence on catalyst nuclearity was seen, and a single catalyst could display both nucleophilic and electrophilic behavior, depending on the substrate.

We and others have evidence that H_2O_2 activation steps are rate limiting for relatively electron-rich substrates [55], which would require little or no dependence of rate on the alkene, consistent with the flat rates between R = H and R = CN. However, for cases where attack of the alkane at the activated H_2O_2 is rate-limiting, the activated H_2O_2 oxidant is electrophilic [56,70], with *higher* rates expected for more electron-donating reactants, in contrast with what is seen here for R = OMe to R = H. This suggests that other effects are at play, such as product inhibition.

The epoxidation of 4-cyanostyrene with **Mn**$_2$/BA-SiO_2 is chosen for a base case of a high-yielding, highly selective reaction to test for rate inhibition by specific functional groups in reactants and products. Table 4 summarizes the initial rates observed with anisole, styrene oxide, styrene diol and benzonitrile added at $t = 0$. Additional nitrile groups from benzonitrile show no significant inhibitory effect, as expected with acetonitrile solvent. 0.1 M anisole (equimolar with alkene) decreases rates 5-fold and yields fall to ca. 70%, suggesting inhibition by the ether group. Assuming a mechanism with relatively weak binding of H_2O_2 and alkene, but stronger binding of an inhibitor, initial rates (r_0) follow Eq. (1):

$$r_0 = \frac{k[\text{alkene}]_0[H_2O_2]_0}{(1 + K_I[\text{inhibitor}]_0)} \quad (1)$$

where concentrations are given in brackets, k is a lumped rate constant, and K_I is the binding constant for each of the inhibitors. Rates relative to the base case with no inhibitor are therefore expressed as Eq. (2):

$$\frac{r_{CN,0}}{r_{I,0}} = 1 + K_I[\text{inhibitor}]_0 \quad (2)$$

The K_I for anisole is of order 10^1–10^2 M^{-1}. At 0.02 M styrene oxide, corresponding to 20% conversion, rates decrease >30-fold, for a K_I of order 10^3 M^{-1}, and epoxide yield falls to ~10%. Styrene diol shows strong inhibitory effects even at 1% of the alkene concentration (0.001 M), or K_I of order 10^4 M^{-1}. Because styrene diol is formed by styrene oxide hydrolysis, it cannot be ruled out that the inhibition by the oxide is, in actuality, inhibition by a small quantity of diol formed under reaction conditions. Overall, it is clear that these catalysts are strongly product-inhibited during styrene oxidation, which has attracted surprisingly little attention in the literature. In contrast, some of us reported earlier that cyclooctane oxide and diol were only weakly inhibitory [55].

Thus, rates of **Mn**$_1$- or **Mn**$_2$- catalyzed epoxidation with H_2O_2 are expected to decrease as the reaction progresses and styrene oxide and diol concentrations increase. Further, electron-rich *p*-X-styrene oxides like that of vinyl anisole, are particularly prone to hydrolyzing to the inhibitory diols [71]. It should be noted that under reaction and analysis conditions, diol manifests itself as the oxidative cleavage product *p*-X-benzaldehyde. In contrast, the electron-poor styrenes are not inhibitory reactants, and they do not as readily form the strongly inhibitory diols, thus giving higher yields.

Overall, these results suggest that **Mn**$_1$ and **Mn**$_2$ operate via similar mechanisms but are indeed different catalysts, supporting mechanistic proposals and structural assignments for a reactive dimeric complex [40,55], and in contrast with mechanisms proposing the dissociation of Mn dimers into monomeric catalysts under reaction conditions [47]. Dissociation of the dimer into two separate, active monomers would require **Mn**$_2$ to have turnover rates approximately twice those of **Mn**$_1$. In fact, we observe that for the BA-SiO_2 co-catalyst, **Mn**$_2$ catalysts are typically 3- to 4-fold faster, and for certain reactants, such as X = CF_3, **Mn**$_2$ is more than an order of magnitude faster than **Mn**$_1$. Thus, while we cannot rule out the possibility that each Mn atom in **Mn**$_2$ acts independently under epoxidation reaction conditions with H_2O_2, where the Mn—O—Mn bond on Scheme 1 will be cleaved, it does appear that these Mn atoms are in a reactive environment different from that formed from immobilization of **Mn**$_1$.

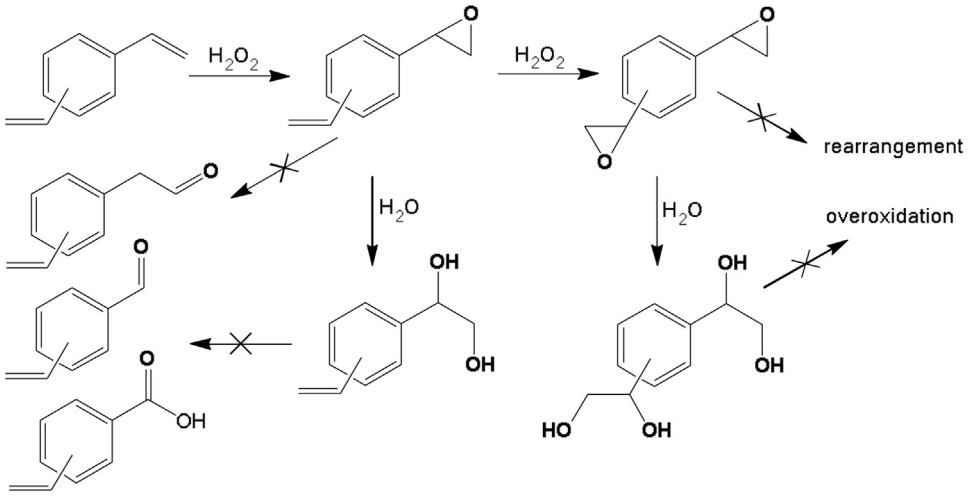

Scheme 4. Divinylbenzene (DVB) epoxidation into divinylbenzene monoxide (DVBMO) and divinylbenzene dioxide (DVBDO)[a].
[a]No further oxidation or rearrangement products of DVBMO, analogous to Scheme 3, are detected. Diols, acid, and other overoxidation products of DVBDO cannot be detected by GC, but are presumed to be present based on mass balance.

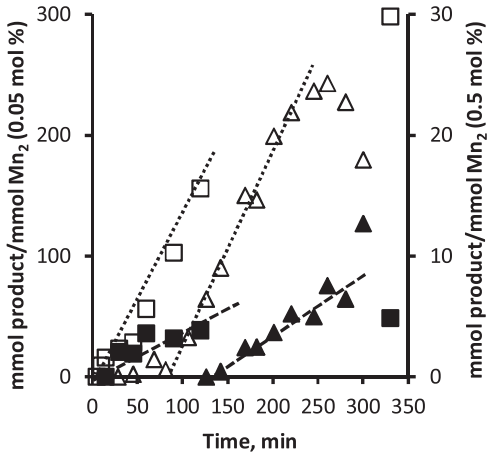

Fig. 3. Representative kinetic profiles for the first 5 h of conversion of DVB into DVBMO (open) and DVBDO (closed), with H_2O_2 as catalyzed by 0.05 mol% (square) or 0.5 mol% (triangle) **Mn**$_2$/BA-SiO_2 with respect to double bonds. Total epoxide selectivity exceeds 90% over this time range. Lines show initial rates for each of the four product/catalyst combinations.

3.4. Catalytic epoxidation of divinylbenzene

Finally, knowledge about supported **Mn**$_1$ and **Mn**$_2$ is applied to the challenging conversion of divinylbenzene (DVB) into the monoxide (DVBMO) and dioxide (DVBDO) (Scheme 4). Fig. 3 shows a representative 5-h kinetic profile for divinylbenzene epoxidation with **Mn**$_2$/BA-SiO_2 at 0.05 and 0.5 mol% **Mn**$_2$ relative to double bond. The induction period following H_2O_2 addition is ~15 min at the low catalyst loading and ~30 min for the high catalyst loading, consistent with slow coordination of **Mn**$_2$ with the co-catalyst/support. The net DVBMO formation rate is greater than the net rate of DVBDO formation at both loadings, and at the higher catalyst loadings, DBVMO passes through a maximum, and the initial DVBDO production rate is zero for nearly 30 min beyond the induction period, consistent with the expected stepwise epoxidation of DVB to DVBMO then to DVBDO.

Table 5 gives initial DVBMO production rates (net) and the % DVB conversion and DVBMO and DVBDO product distributions at 24 h. Initial rates are calculated from sustained initial rates of DVBMO formation and neglect induction periods of ~15 min in most cases. Negligible amounts of DVBMO overoxidation or rearrangement products (monofunctional acids and aldehydes) were detected, implying that similar (but undetectable by the GC) side products from DVBDO were also likely absent. Glycols of DVB are not able to be detected by GC due to strong interactions with all columns and the absence of suitable capping agents that are also unreactive with the epoxide. Glycol selectivity was thus inferred from the difference in DVB consumed and DVBMO and DVBDO produced. This is an upper bound for the amount of glycols produced, as DVBMO and DVBDO do adsorb to functionalized silica surfaces (Supporting information Fig. S6).

At conditions comparable to those of Table 3 and Fig. 2, initial rates of DVBMO synthesis for **Mn**$_1$ and **Mn**$_2$/BA-SiO_2 (Table 4, entries 3 and 13) are lower than those of those of styrene, consistent with a weakly-donating vinyl fragment ($\sigma_p = -0.02$) [65]. The epoxide on DVBMO is more electron-donating, which explains the further rate depression, relative to styrene, for catalysts like **Mn**$_2$/BA-SiO_2 that have higher DBVDO selectivities. This suggests that pushing to high yields of DVBDO is particularly challenging, which is borne out by the high (undesired) glycol selectivities at high DVB conversion for many entries in Table 5.

At the baseline conditions (entries 1, 2, 10, 11), **Mn**$_2$/BA-SiO_2 gives the best overall performance, as it does for the monofunctional styrenes, with 19% DVBDO selectivity at 54% DVB conversion, and no significant glycol production. These materials are then optimized to increase DVBDO yields. Increasing the H_2O_2 concentration (entry 12) maintains rates, increases DVB conversion and DVBDO selectivity, but results in significant hydrolysis to glycols. Increasing the catalyst loading (entries 3, 13, 15, 16) increases DVB conversion to as high as 97%. Initial TOF decreases with increasing catalyst loading, suggesting that initial catalyst activation is limited by the available H_2O_2. DVBDO selectivity increases appreciably, but hydrolysis also increases and becomes the largest product.

These results highlight the need for maintaining low oxidant and catalyst concentrations throughout the reaction to minimize glycol formation. As an alternate approach, a cascade of batch reactors was employed. (entries 3 → 4, 13 → 14). After one reaction period, the reaction solution is decanted from the catalyst and added to a reactor containing fresh catalyst, co-catalyst, and charge of H_2O_2. An example reaction profile is given in Supporting Information Fig. S7. Entries 4 (**Mn**$_1$) and 14 (**Mn**$_2$) show >95% DVB conversion, with DVBDO yields of 74% and 55%, respectively. The **Mn**$_1$ system is particularly effective when used in this manner, since it minimizes the extent of hydrolysis.

Table 5
Summary of DVB conversion, product selectivity (% DVBDO, DVBMO, and inferred glycols) and initial rates for DVBMO production with H_2O_2 over several catalytic systems.[a]

	Catalyst loading[b]	DVB Conv.	Product selectivity[c]	Initial rate[d]
1 Mn_1/PA-SiO_2	0.05	41%	5, 95, 0	1.04
2 Mn_1/BA-SiO_2	0.05	32%	5, 95, 0	1.23
3 Mn_1/BA-SiO_2	0.1	45%	10, 77, 13	0.42
4 Mn_1/BA-SiO_2[e]	0.1	96%	77, 10, 13	0.14[e]
5 Mn_1/sol–gel	0.05	39%	38, 53, 9	0.2
6 Mn_1/C	0.1	18%	4, 96, 0	0.47
7 Mn_1/C[e]	0.1	56%	19, 81, 0	0.5[e]
8 Mn_1/AC	0.1	53%	8, 76, 16	1.73
9 Mn_1/AC[e]	0.1	77%	20, 46, 34	0.34[e]
10 Mn_2/PA-SiO_2	0.05	58%	16, 73, 11	1.28
11 Mn_2/BA-SiO_2	0.05	54%	19, 81, 0	1.27
12 Mn_2/BA-SiO_2[f]	0.05	69%	18, 38, 44	1.37
13 Mn_2/BA-SiO_2	0.1	67%	22, 58, 20	0.51
14 Mn_2/BA-SiO_2[e]	0.1	>99%	55, 5, 40	-0.15[e]
15 Mn_2/BA-SiO_2	0.25	73%	9, 35, 56	0.36
16 Mn_2/BA-SiO_2	0.5	97%[g]	35, 6, 58[g]	0.16
17 Mn_2/sol–gel	0.05	49%	26, 49, 25	0.14
18 Mn_2/C	0.1	17%	15, 85, 0	0.19
19 Mn_2/C[e]	0.1	45%	10, 77, 7	0.39[e]
20 Mn_2/AC	0.1	70%	25, 75, 0	1.58
21 Mn_2/AC[e]	0.1	98%	40, 11, 49	-0.19[e]

[a] Conditions: 0.1 M divinylbenzene, 0.3 M dried H_2O_2/MeCN, 10:1 supported acid:Mn center, 0 °C, MeCN. 0.4 mg carbons supports per mL solution. conversion and selectivity at 24 h.
[b] mole% **Mn_1** or **Mn_2** with respect to double bonds in DVB.
[c] Product selectivity as%DVBDO,%DVBMO, and% total glycols. The latter is inferred from the difference between DVB consumed and DVBDO and DVBMO observed.
[d] Net initial rate (mmol DVBMO/mmol **Mn_1** or **Mn_2**/min).
[e] Reaction supernatant from above entry was added to fresh catalyst, co-catalyst, and 1.5 eq. H_2O_2 per double bond. Low or negative rates indicate consumption of DVBMO from the prior run.
[f] 0.5 M H_2O_2 in reaction mixture.
[g] Reported values at t = 2 h.

Using these optimized conditions, two additional classes of supports were examined: a co-condensed organosilica giving high loadings of a butanoic acid (Scheme 2) and a high surface area carbon (C, Table 1). The sol–gel material (entries 5, 17) gives comparable conversions as PA-SiO_2 (entries 1, 10), consistent with their similar structures, but the higher acid density gives rise to much higher DVBDO selectivity, and, unfortunately, higher extents of hydrolysis.

Carbon co-catalysts were proposed as analogues of the successful BA-SiO_2 materials, given the presence of oxygen defects on an extended pi surface. The parent carbon gives only modest conversions and DVBDO selectivity, even after a two-reactor cascade (entries 6, 7, 18, 19). To increase the number of available carboxylates, the carbons were further treated with HNO_3 and used again. The acid-treated carbons (AC) give significantly higher DVB conversion and DVBDO selectivity (entries 8, 9, 20, 21), but also see significant hydrolysis to glycols. On the first reaction cycle, the acid-treated carbons give quite similar product distributions to BA-SiO_2, justifying the hypothesis regarding their similar structures. However, the acid-treated carbons do not give the same improvements in DVBDO yield with a second reactor in series.

4. Summary and conclusions

To the best of our knowledge, this is the first systematic comparison of the activities of supported 'non-heme' catalysts of different nuclearity, e.g., **Mn_1** and **Mn_2**, as catalysts for alkene epoxidation with H_2O_2. We find that the immobilized benzoic acid co-catalyst (BA-SiO_2) give higher yields than an immobilized propanoic acid, apparently due to enhanced resistance to deactivation and inhibition. The Hammett analysis of *p*-substituted styrene epoxidation with **Mn_1** or **Mn_2** and the BA-SiO_2 co-catalyst gives support for a rate limiting step before the epoxidation step (e.g., H_2O_2 activation) but also for confounding effects from product inhibition. In particular, we propose strong inhibition by even 1% (with respect to alkene) styrene diol. Thus, the more electron-rich styrenes like vinyl anisole (methoxystyrene), whose oxide product is readily hydrolyzed into diol, are intrinsically challenging to drive to high conversion over these systems, due to strong product inhibition. Thus, an advantage of the immobilized system is the ability to operate in series reactors or in a packed bed of catalyst—geometries that help minimize product inhibition. We demonstrate that even a simple two-reactor series can drive the important and challenging epoxidation of DVB to ~75% yield of divinylbenzene dioxide (DVBDO). In any reactor configuration, these catalysts seem very well suited for epoxidation with less electron-rich alkenes, complementing traditional epoxidation catalysts like Ti-SiO_2 that perform better with electron-rich alkenes. In general, particular care must be taken in the interpretation of the kinetics of this system due to strong effects of catalyst nuclearity, co-catalyst, and reactant electronics on intrinsic rate, permanent catalyst deactivation, and reactant/product inhibition.

Acknowledgements

The authors acknowledge financial assistance from The Dow Chemical Company and thank Dr. Kurt Hirsekorn and Dr. Nicholas Schoenfeldt for helpful discussions. A.B.T. also acknowledges financial support from NSF grant CBET-0933667. SS ^{13}C CP/MAS NMR spectroscopy was performed at IMSERC, funded by NSF DMR-0521267. SEM and DRIFTS experiments were carried out at NUANCE with support from NSF-NSEC, NSF-MRSEC, Keck Foundation, the State of Illinois and Northwestern University.

Appendix A. Supplementary data

Supplementary data associated with this article can be found, in the online version, at http://dx.doi.org/10.1016/j.apcata.2015.12.002.

References

[1] M. Fujita, L. Que, Adv. Synth. Catal. 346 (2004) 190–194.
[2] S. Yamabe, C. Kondou, T. Minato, J. Org. Chem. 61 (1996) 616–620.
[3] P.A. Lichtor, S.J. Miller, Nat. Chem. 4 (2012) 990–995.
[4] Y.Y. Chu, X.H. Liu, W. Li, X.L. Hu, L.L. Lin, X.M. Feng, Chem. Sci. 3 (2012) 1996–2000.
[5] B. Qi, X.H. Lu, D. Zhou, Q.H. Xia, Z.R. Tang, S.Y. Fang, T. Pang, Y.L. Dong, J. Mol. Catal. A—Chem. 322 (2010) 73–79.
[6] B.S. Lane, K. Burgess, Chem. Rev. 103 (2003) 2457–2474.
[7] R.I. Kureshy, T. Roy, N.U. Khan, S.H.R. Abdi, A. Sadhukhan, H.C. Bajaj, J. Catal. 286 (2012) 41–50.
[8] W. Zhang, J.L. Loebach, S.R. Wilson, E.N. Jacobsen, J. Am. Chem. Soc. 112 (1990) 2801–2803.
[9] W. Zhang, E.N. Jacobsen, J. Org. Chem. 56 (1991) 2296–2298.
[10] T. Katsuki, Adv. Synth. Catal. 344 (2002) 131–147.
[11] J.P. Renaud, P. Battioni, J.F. Bartoli, D. Mansuy, J. Chem. Soc. Chem. Comm. (1985) 888–889.
[12] D. Mansuy, P. Battioni, J.P. Renaud, P. Guerin, J. Chem. Soc. Chem. Comm. (1985) 155–156.
[13] L.J. Boucher, J. Am. Chem. Soc. 90 (1968) 6640–6645.
[14] N.J. Schoenfeldt, Z.J. Ni, A.W. Korinda, R.J. Meyer, J.M. Notestein, J. Am. Chem. Soc. 133 (2011) 18684–18695.
[15] M. Costas, K. Chen, L. Que, Coord. Chem. Rev. 200 (2000) 517–544.
[16] M.H. Lim, J.U. Rohde, A. Stubna, M.R. Bukowski, M. Costas, R.Y.N. Ho, E. Munck, W. Nam, L. Que, Proc. Natl. Acad. Sci. U. S. A. 100 (2003) 3665–3670.
[17] M. Costas, A.K. Tipton, K. Chen, D.H. Jo, L. Que, J. Am. Chem. Soc. 123 (2001) 6722–6723.
[18] M. Ostermeier, C. Limberg, C. Herwig, B. Ziemer, Z. Anorg. Allg. Chem. 635 (2009) 1823–1830.
[19] S.D. Zhou, X.Z. Chen, C. Qian, Chem. Phys. Lett. 488 (2010) 44–49.
[20] J. Huang, X.K. Fu, G. Wang, Y.Q. Ge, Q. Miao, J. Mol. Catal. A—Chem. 357 (2012) 162–173.
[21] I. Kuzniarska-Biernacka, A.R. Silva, A.P. Carvalho, J. Pires, C. Freire, Catal. Lett. 134 (2010) 63–71.
[22] K. Weighardt, U. Bossek, B. Nuber, J. Weiss, J. Bonvoisin, M. Corbella, S.E. Vitols, J.J. Girerd, J. Am. Chem. Soc. 110 (1988) 7398–7411.
[23] W.R. Browne, J.W. de Boer, D. Pijper, J. Brinksma, R. Hage, B.L. Feringa, Modern Oxidation Methods, in: J.E. Backvall (Ed.), Wiley-VCH, Germany, 2010, pp. 371–419.
[24] P. Saisaha, J.W. de Boer, W.R. Browne, Chem. Soc. Rev. 42 (2013) 2059–2074.
[25] R. Hage, J.E. Iburg, J. Kerschner, J.H. Koek, E.L.M. Lempers, R.J. Martens, U.S. Racherla, S.W. Russell, T. Swarthoff, M.R.P. Vanvliet, J.B. Warnaar, L. Vanderwolf, B. Krijnen, Nature 369 (1994) 637–639.
[26] V.C. QueeSmith, L. DelPizzo, S.H. Jureller, J.L. Kerschner, R. Hage, Inorg. Chem. 35 (1996) 6461–6465.
[27] D. DeVos, T. Bein, Chem. Commun. (1996) 917–918.
[28] C. Zondervan, R. Hage, B.L. Feringa, Chem. Commun. (1997) 419–420.
[29] A. Berkessel, C.A. Sklorz, Tetrahedron Lett. 40 (1999) 7965–7968.
[30] B.C. Gilbert, N.W.J. Kamp, J.R.L. Smith, J. Oakes, J. Chem. Soc. Perkin Trans. 2 (1997) 2161–2166.
[31] D.H.R. Barton, S.Y. Choi, B. Hu, J.A. Smith, Tetrahedron 54 (1998) 3367–3378.
[32] J.H. Koek, E.W.M.J. Kohlen, S.W. Russell, L. van der Wolf, P.F. ter Steeg, J.C. Hellemons, Inorg. Chim. Acta 295 (1999) 189–199.
[33] J.E. Barker, T. Ren, Tetrahedron Lett. 45 (2004) 4681–4683.
[34] J.R.L. Smith, G.B. Shul'pin, Tetrahedron Lett. 39 (1998) 4909–4912.
[35] G.B. Shul'pin, G. Suss-Fink, J.R.L. Smith, Tetrahedron 55 (1999) 5345–5358.
[36] T.H. Bennur, S. Sabne, S.S. Deshpande, D. Srinivas, S. Sivasanker, J. Mol. Catal. A—Chem. 185 (2002) 71–80.
[37] D. Mandelli, Y.N. Kozlov, W.A. Carvalho, G.B. Shul'pin, Catal. Commun. 26 (2012) 93–97.
[38] G.B. Shul'pin, G. Suss-Fink, L.S. Shul'pina, J. Mol. Catal. A 170 (2001) 17–34.
[39] J.W. de Boer, J. Brinksma, W.R. Browne, A. Meetsma, P.L. Alsters, R. Hage, B.L. Feringa, J. Am. Chem. Soc. 127 (2005) 7990–7991.
[40] J.W. de Boer, W.R. Browne, J. Brinksma, P.L. Alsters, R. Hage, B.L. Feringa, Inorg. Chem. 46 (2007) 6353–6372.
[41] R. Hage, A. Lienke, Angew. Chem. Int. Edit. 45 (2006) 206–222.
[42] K.F. Sibbons, K. Shastri, M. Watkinson, Dalton Trans. (2006) 645–661.
[43] M. Verrall, Nature 369 (1994) 511.
[44] M. Verrall, Nature 373 (1995) 181.
[45] J. Brinksma, L. Schmieder, G. van Vliet, R. Boaron, R. Hage, D.E. De Vos, P.L. Alsters, B.L. Feringa, Tetrahedron Lett. 43 (2002) 2619–2622.
[46] V.B. Romakh, B. Therrien, L. Karmazin-Brelot, G. Labat, H. Stoeckli-Evans, G.B. Shul'pin, G. Suss-Fink, Inorg. Chim. Acta 359 (2006) 1619–1626.
[47] D.E. De Vos, S.D. Wildeman, B.F. Sels, P.J. Grobet, P.A. Jacobs, Angew. Chem. Int. Edit. 38 (1999) 980–983.
[48] F.S. Vinhado, C.M.C. Prado-Manso, H.C. Sacco, Y. Iamamoto, J. Mol. Catal. A—Chem. 174 (2001) 279–288.
[49] P.R. Cooke, J.R.L. Smith, Tetrahedron Lett. 33 (1992) 2737–2740.
[50] P.R. Cooke, J.R.L. Smith, J. Chem. Soc. Perkin Trans. 1 (1994) 1913–1923.
[51] Y.V.S. Rao, D.E. DeVos, T. Bein, P.A. Jacobs, Chem. Commun. (1997) 355–356.
[52] M. Bosch, D. Veghini, Manganese(IV) complex salts and their use as oxidation catalysts, US Patent 7,034,170, (2006).
[53] N.J. Schoenfeldt, A.W. Korinda, J.M. Notestein, Chem. Commun. 46 (2010) 1640–1642.
[54] N.J. Schoenfeldt, J.M. Notestein, ACS Catal. 1 (2011) 1691–1701.
[55] K.R. Bjorkman, N.J. Schoenfeldt, J.M. Notestein, L.J. Broadbelt, J. Catal. 291 (2012) 17–25.
[56] B.C. Gilbert, J.R.L. Smith, A.M.I. Payeras, J. Oakes, Org. Biomol. Chem. 2 (2004) 1176–1180.
[57] G. Ilyashenko, G. De Faveri, S. Masoudi, R. Al-Safadi, M. Watkinson, Org. Biomol. Chem. 11 (2013) 1942–1951.
[58] G.H. Searle, R.J. Geue, Aust. J. Chem. 37 (1984) 959–970.
[59] J.A. Elings, R. Ait-Meddour, J.H. Clark, D.J. Macquarrie, Chem. Commun. (1998) 2707–2708.
[60] R. Mello, A. Alcalde-Aragones, M.E.G. Nunez, G. Asensio, J. Org. Chem. 77 (2012) 6409–6413.
[61] A. Lambert, J.A. Elings, D.J. Macquarrie, G. Carr, J.H. Clark, Synlett 7 (2000) 1052–1054.
[62] A. Mello, A. Alcalde-Aragones, M.E.G. Diaz-Rodriguez, G. Asensio, Eur. J. Org. Chem. 75 (2010) 6200–6206.
[63] R. Mello, A. Olmos, J. Parra-Carbonell, M.E. Gonzalez-Nunez, G. Asensio, Green Chem. 11 (2009) 994–999.
[64] J.P. Collman, T. Kodadek, J.I. Brauman, J. Am. Chem. Soc. 108 (1986) 2588–2594.
[65] G. Saul Cohen, Andrew Streitwieser Jr., W. Robert Taft (Eds.), Progress in Physical Organic Chemistry, vol. 2, Interscience Publishers, a division of John Wiley & Sons, New York, 1964.
[66] J.A. Dean, Lange's Handbook of Chemistry, 13th ed., McGraw-Hill, New York, 1985.
[67] G.B. Shul'pin, M.G. Matthes, V.B. Romakh, M.I.F. Barbosa, J.L.T. Aoyagi, D. Mandelli, Tetrahedron 64 (2008) 2143–2152.
[68] D.D. Perrin, B. Dempsey, E.P. Serjeant, pK_a Prediction for Organic Acids and Bases, Chapman and Hall, New York, 1981.
[69] R. Mello, A. Alcalde-Aragones, A. Olmos, M.E. Gonzalez-Nunez, G. Asensio, J. Org. Chem. 77 (2012) 4706–4710.
[70] I. Garcia-Bosch, A. Company, X. Fontrodona, X. Ribas, M. Costas, Org. Lett. 10 (2008) 2095–2098.
[71] J.J. Blumenstein, V.C. Ukachukwu, R.S. Mohan, D.L. Whalen, J. Org. Chem. 58 (1993) 924–932.
[72] Q. Feng, Q.L. Song, J. Org. Chem. 79 (2014) 1867–1871.